Electronic Supplementary Information (ESI)

Supramolecular assemblies of Cu(II) with tetraphenylethene-imidazole ligand for tuning photocatalytic CO_2 reduction

Zhao-Feng Qiu, Peng Wang, Xiao-Yu Zhang, Jia-Qi Chen, Kai-Yang Zhang, Xiang-Yu Lu, Yue Zhao and Wei-Yin Sun*

Coordination Chemistry Institute, State Key Laboratory of Coordination Chemistry, School of Chemistry and Chemical Engineering, Nanjing National Laboratory of Microstructures, Collaborative Innovation Center of Advanced Microstructures, Nanjing University, Nanjing, 210023, China

*Corresponding author

E-mail: sunwy@nju.edu.cn.

Materials and methods.

All commercial chemicals and solvents are reagent grade and were used without further purification, tipe ligand was synthesized with reference to the published work.[1, 2] Powder X-ray diffraction (PXRD) data were obtained on a Bruker D8 Advance X-ray diffractometer with Cu Kα radiation (1.5478 Å) at 40 kV and 40 mA over the 2θ range of 5-50°. UV-Vis diffuse reflectance spectra (DRS) were carried out on a Shimadzu UV-3600 spectrophotometer in the wavelength range of 200-1000 nm. A Elementar UNICUBE elemental analyzer was used to attain elemental analyses of C, H, and N. All gas adsorption isotherms were obtained by employing a standard volumetric technique up to saturated pressure on a Micromeritics ASAP 2020 volumetric gas sorption analyzer. Photoluminescence (PL) spectra were measured on PerkinElmer LS-55 spectrofluorometer with a xenon lamp as a light source. Thermogravimetric analysis (TGA) was carried out on Mettler Toledo thermal analyser at a temperature of 10 °C/min under nitrogen. Fourier-transform infrared spectra (FT-IR, KBr pellets) were recorded on Bruker Vector 22 FT-IR spectrometer from 4000 to 400 cm^{-1}. ^1H NMR spectra were acquired on Bruker-DRX 400 MHz instruments at room temperature in D_2O. *In situ ATR-*

SEIRAS (Attenuated total reflectance surface-enhanced infrared absorption spectroscopy) tests were performed using iS50R Full Band Research Grade Infrared Spectroscopy Workstation equipped with an MCT detector. Cu-MOF (5 mg) catalyst was subjected to MeCN/H_2O (v:v = 4:1, 20 ml), $[Ru(bpy)_3]Cl_2 \cdot 6H_2O$ (0.02 mmol) and triisopropanolamine (TIPA) (9.4 mmol) in CO_2 atmosphere under 300 W xenon lamp irradiation. Time-dependent in situ diffuse reflectance FT-IR spectra were collected within every 10 min in the dark (background) and under xenon lamp irradiation

Synthesis of $[Cu_2(tipe)_2(H_2O)_2](NO_3)_4 \cdot 2.5H_2O$ (CuN_4). Ligand tipe (0.02 mmol, 12.0 mg) and $Cu(NO_3)_2 \cdot 3H_2O$ (0.10 mmol, 24.1 mg) were ultrasonically dissolved in 4 mL mixed solvent of CH_3CN/H_2O (v:v = 4:1) in a 10 mL pressure resistant glass bottle. Then $NH_3 \cdot H_2O$ (50 μL) was added to this solution. The reaction system was heated at 120 °C for 72 h in a programmed oven. After gradually cooling to room temperature, blue block crystals were isolated (Yield: 74%, based on tipe). Anal. Calcd for $C_{76}H_{65}Cu_2N_{20}O_{16.5}$: C, 55.34; H, 3.94; N, 16.99. Found: C, 56.12; H, 3.71; N, 17.36.

Synthesis of $[Cu_2Cl_4(tipe)(CH_3CN)] \cdot H_2O$ (CuN_2Cl_2). Tipe (0.04 mmol, 24.0 mg) and $CuCl_2 \cdot 2H_2O$ (0.10 mmol, 17.0 mg) were dissolved in 4 mL mixed solvent of CH_3CN/H_2O (v:v = 4:1) in a 10 mL pressure resistant glass bottle. Then 40 μL of dilute nitric acid was added to the solution. Reaction temperature and time were the same as **CuN_4**, green needle crystals were obtained (Yield: 51%, based on tipe). Anal. Calcd for $C_{40}H_{33}Cl_4Cu_2N_9O$: C, 51.96; H, 3.60; N, 13.63. Found: C, 52.02; H, 3.67; N, 13.60.

X-ray crystallography.

Single-crystal X-ray diffraction data were collected on a Bruker D8 Venture diffractometer with a graphite-monochromated Ga Kα radiation (λ = 1.34139 Å) at 193 K. The integration of diffraction data and intensity corrections for the Lorentz and polarization effects were performed by using the SAINT program.[3] Semi-empirical absorption corrections were applied using the SADABS program.[4] The structures were computed by direct methods with SHELXT-2014, expanded by subsequent Fourier-difference synthesis, and all the non-hydrogen atoms were refined anisotropically on F^2 using the full-matrix least-squares technique using the SHELXL-2018 crystallographic software package.[5] In **CuN_4**, the hydrogen atoms were calculated geometrically and refined isotropically using the riding model, while those of water

molecules were found directly. In this heavy-atom structure as it was not possible to see clear electron-density peaks in difference-map plots which would correspond with acceptable locations for the various H atoms bonded to water oxygen atoms, the refinement was completed with no allowance for these water H atoms in the model. In Cu-Cl, the hydrogen atoms were calculated geometrically and refined isotropically using the riding model, while those of water molecules were found directly. Crystal data and refinement details of **CuN_4** and **CuN_2Cl_2** are given in Table S1, selected bond lengths and angles are listed in Tables S2 and S3.

Electrochemical tests.

Mott-Schottky test was conducted using the Zahner electrochemical workstation in a typical three-electrode configuration. The working electrode was catalyst-coated glassy carbon, while the counter electrode was a Pt wire, and the reference electrode was an Ag/AgCl. The electrolyte was 0.2 M Na_2SO_4 solution. To prepare the ink, 5 mg of catalyst and 20 μL of Nafion (Du Pont) were added to 1 ml of isopropanol and subjected to ultrasonic processing. The 200 μL ink was then dropped onto the ITO of the working electrode and dried under an infrared lamp to form a tightly packed layer. The measurements were conducted at frequencies of 500, 1000 and 1500 Hz.

Electrochemical impedance spectroscopy (EIS) was undertaken at Zahner electrochemical workstation in a 0.2 M Na_2SO_4 solution using a three-electrode system. The reference and counter electrodes were Ag/AgCl and Pt plates. 5 mg of synthetic sample was dispersed in a solution containing 20 μL Nafion and 1.0 mL isopropanol. The working electrode was prepared by dropping the above ink (200 μL) onto the surface of the carbon paper and dried at 120 ºC. EIS measurement was performed with a bias potential of -0.1 V with a frequency range from 10^{-2} to 10^5 Hz at room temperature.

Photocurrent measurements were registered on a CHI 730E electrochemical workstation, using a photocatalyst (200 μL) drop prepared by the above method in ITO as the working electrode. Measurements were carried out under a 0.5 V current interval of 20 s of chopped light. Subsequently, the above-prepared ITO working electrode was immerged in $[Ru(bpy)_3]Cl_2 \cdot 6H_2O$ solution (1.33 mM, 1.5 mL) for 1 h and then the photocurrent was measured.

Photocatalytic reactions.

To determine the photocatalytic activity of Cu-MOFs, fresh samples were activated and then used as photocatalysts. The solvent molecules in the pores were swapped out with ethanol and the coordinated solvent molecules in the two Cu-MOFs were removed under vacuum at 80 °C for 6 h. Catalyst (5 mg) and $[Ru(bpy)_3]Cl_2 \cdot 6H_2O$ (bpy = 2,2'-bipyridine, 0.02 mmol) and 9.4 mmol TIPA were added in the 20 ml mixed solution ($MeCN/H_2O$ = 4:1) at 4 ºC. After three complete system evacuations with no detection of N_2 or O_2, ultra-pure CO_2 (99.999%) was introduced at a pressure of 0.8 Mpa. The system was irradiated with a 300 W xenon lamp and with an AM 1.5 G filter (CeAulight) for 5 hours. A gas chromatograph (GC, 9720II) with a TCD detector and FID detector was operated to monitor the gas products during the reaction and the liquid products were monitored by means of ^1H NMR. The turnover number (TON) is defined as the number of produced products that occur per catalyst (Equation S1).

$$TON = \frac{Y_{(CO+H_2)} \times M_{catalyst}}{m_{catalyst}} \qquad \text{Equation S1}$$

In the formula, Y(CO) and $Y(H_2)$ are the yields of CO and H_2, $M_{catalyst}$ is the molecular weight of the catalyst ($M_{\mathbf{CuN2Cl2}}$: 865.56, $M_{\mathbf{CuN4}}$: 1568.56), $m_{catalyst}$ is 5 mg. Therefore, the TON of $\mathbf{CuN_2Cl_2}$ and $\mathbf{CuN_4}$ are 0.035 and 0.35, respectively.

Computational method.

All density functional theory (DFT) calculations were carried out using the Vienna ab initio simulation package (VASP) based on the projector augmented wave (PAW) method. Within the generalized gradient approximation (GGA), the PerdewBurke-Ernzerhof (PBE), a popular exchange-correlation functional, was employed in geometry optimizations.[6] To study the CO_2RR pathway in the MOFs, we built a model in periodic boundary condition (PBC) with the primitive cell. The Grimme method was also applied to take the long-range dispersion interaction into consideration. The kinetic energy cutoff for the plane-wave expansion was set to be 450 eV and a 1×1×1 sheet k-point mesh was used. The Hubbard-like DFT+U approach was used to treat the Cu atom with the effective Ueff. The energy convergence value between two consecutive steps was chosen as 1×10^{-5} eV, and a maximum force was set to be lower than 0.04 eV/Å on each atom. The electrocatalytic mechanisms were studied based on Nöskov's computational hydrogen electrode model.[7]

The CO_2 reduction process can be described by the following steps:

$$* + CO_2 + H^+ + e^- \rightarrow *COOH \qquad (1)$$

$$*COOH + H^+ + e^- \rightarrow *CO + H_2O \qquad (2)$$

$$*CO \rightarrow * + CO \quad (3)$$

The asterisk * represents the adsorption over the catalytic center. The values for the free energies of each gaseous and adsorbed species are calculated by:

$$G = E_{total} + E_{ZPE} - TS \quad (4)$$

E_{total} is the total energy from the DFT calculations. E_{ZPE} is the zero-point energy, S is the entropy, and T is the temperature.

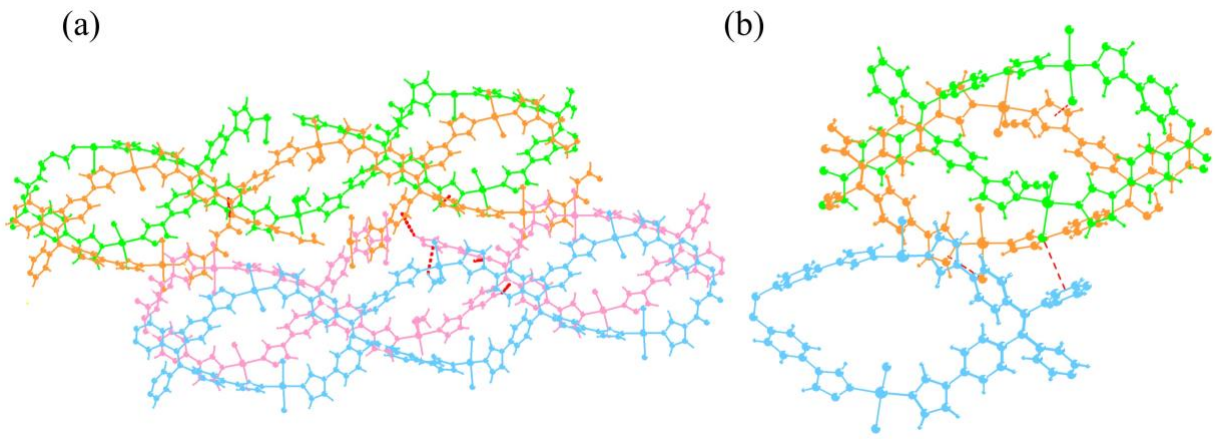

Fig. S1 3D supramolecular structure of **CuN_2Cl_2** constructed with the assistance of hydrogen bonds (a) and p···π interactions (b).

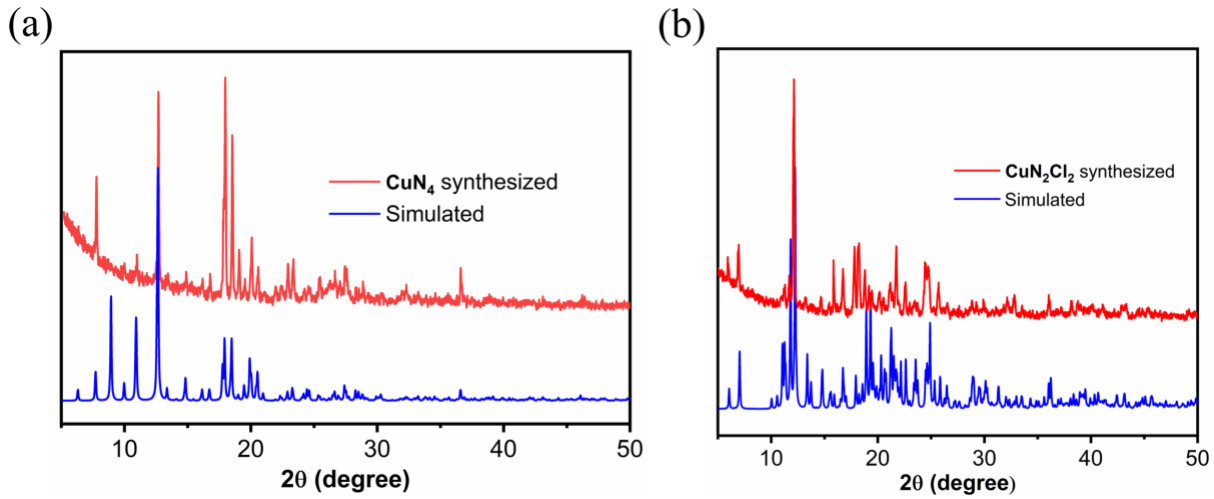

Fig. S2 PXRD of **CuN_4** (a) and **CuN_2Cl_2** (b).

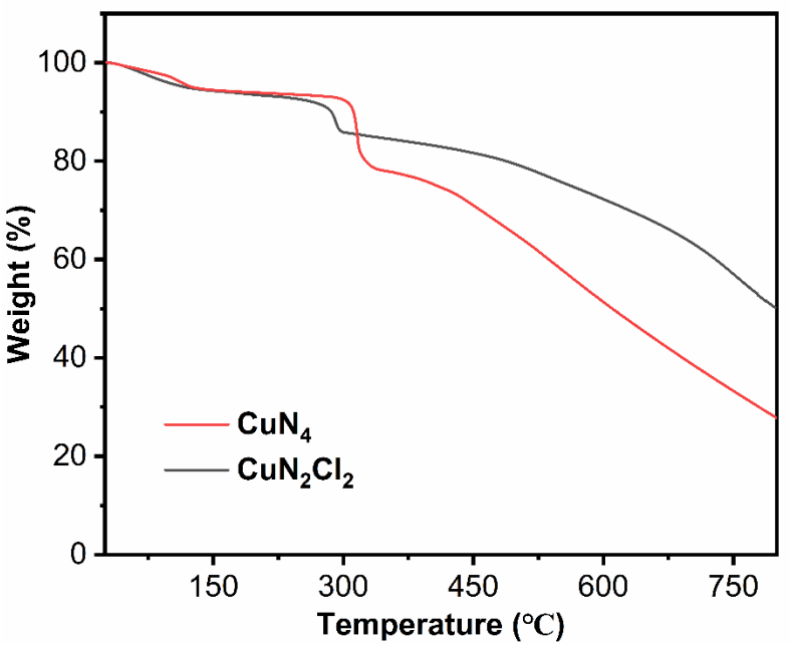

Fig. S3 TG curves of **CuN_4** and **CuN_2Cl_2**.

For **CuN_4**, a weight loss of 5.02 % (calculated as 4.91%) was observed in the range of 25-128 °C due to the loss of coordinated and free water molecules and the decomposition of the residue is up to 310 °C. TG data of **CuN_2Cl_2** indicate weight loss of 5.41% (calculated as 6.38%) in 25-132 °C, which was caused by the departure of free water and coordinated acetonitrile molecules. The supramolecular structure is thermally stable up to 270 °C.

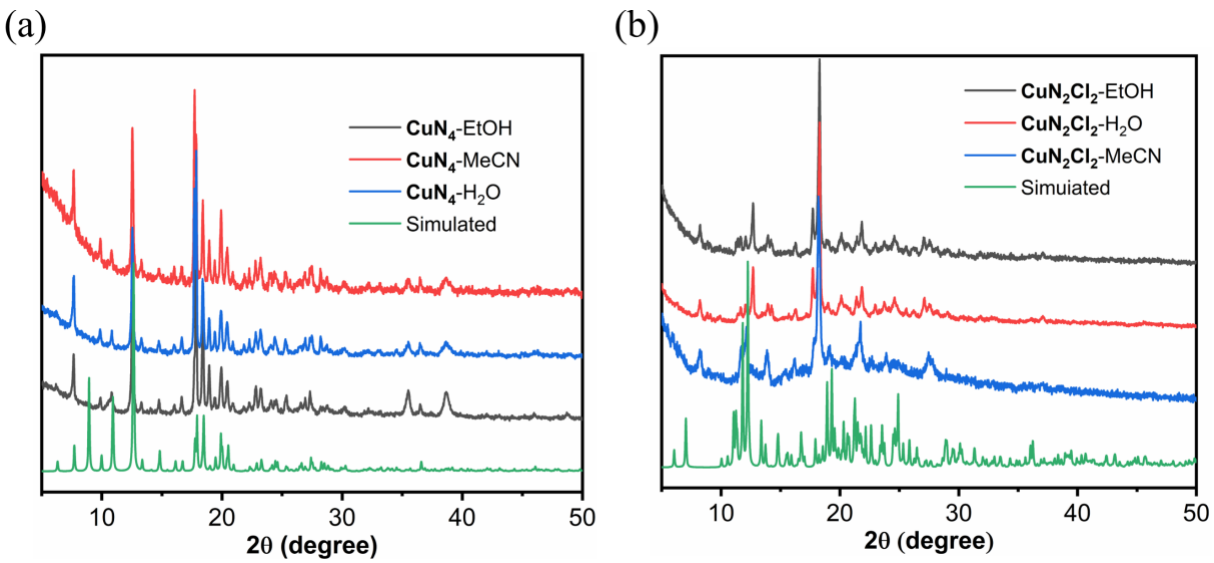

Fig. S4 PXRD of **CuN_4** (a) and **CuN_2Cl_2** (b) in common solvent.

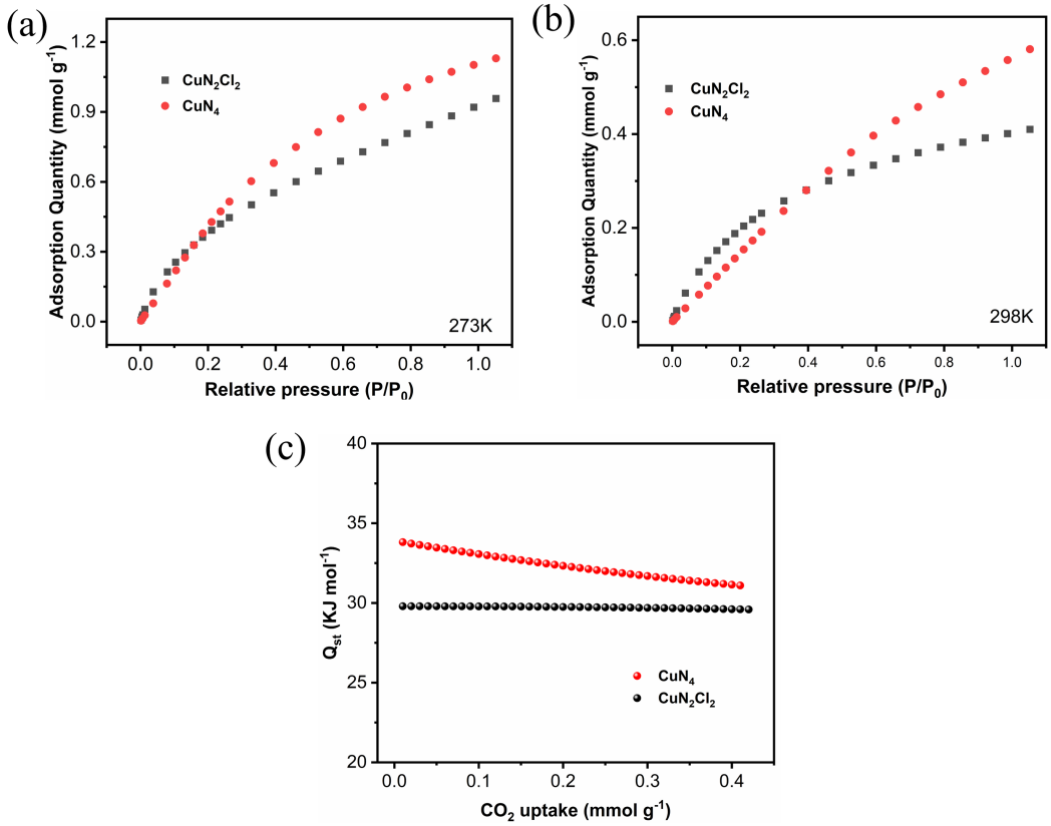

Fig. S5 CO_2 adsorption isotherms of the **CuN_2Cl_2** and **CuN_4** at 273 K (a) and 298 K (b). (c) The CO_2 adsorption enthalpy of **CuN_2Cl_2** and **CuN_4**.

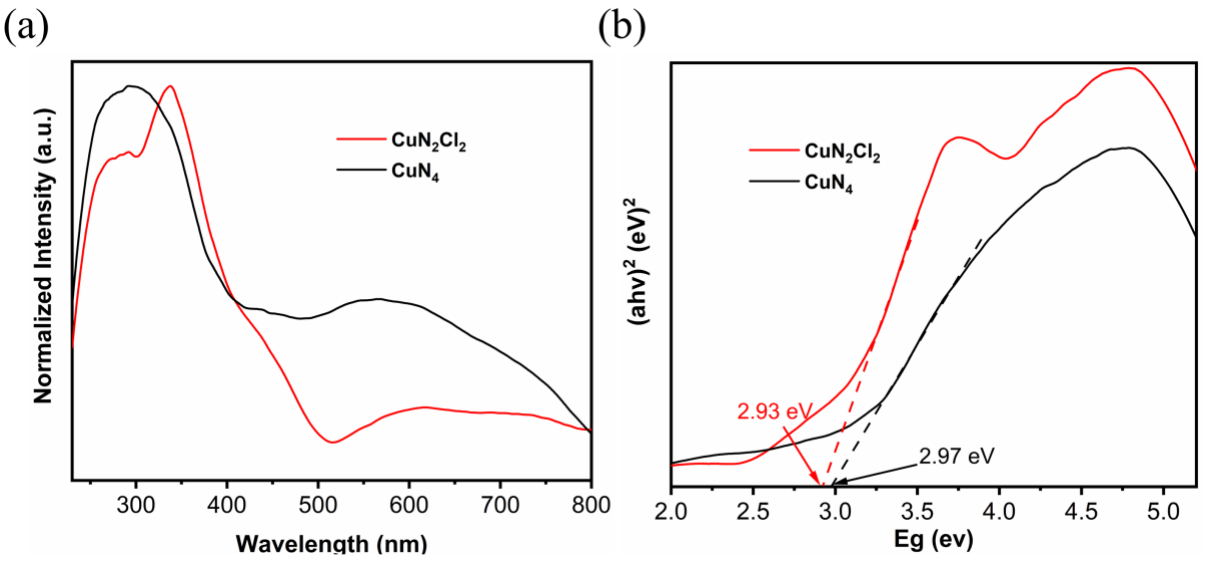

Fig. S6 (a) UV-vis diffuse reflectance spectra of Cu-MOFs. (b) Tauc plots of **CuN_2Cl_2** and **CuN_4**.

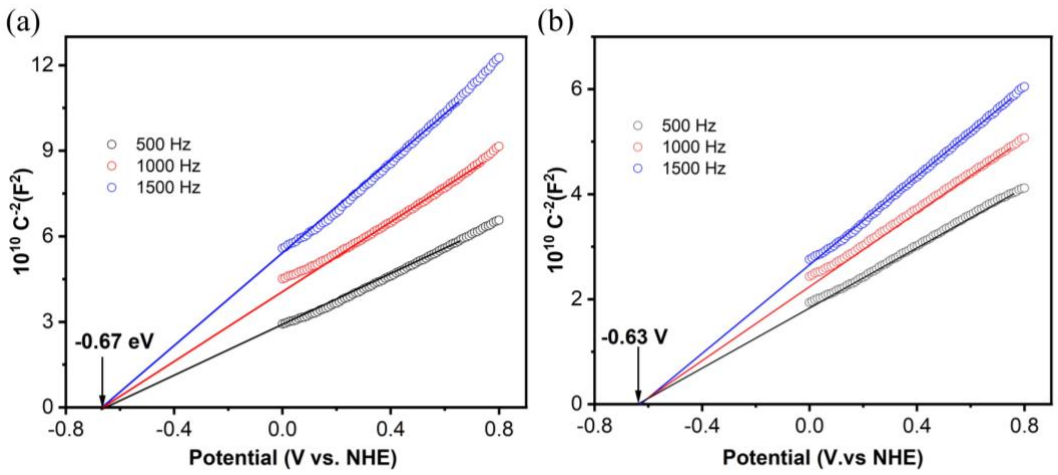

Fig. S7 (a) Mott-Schottky plot of **CuN_2Cl_2**. (b) Mott-Schottky plot of **CuN_4**.

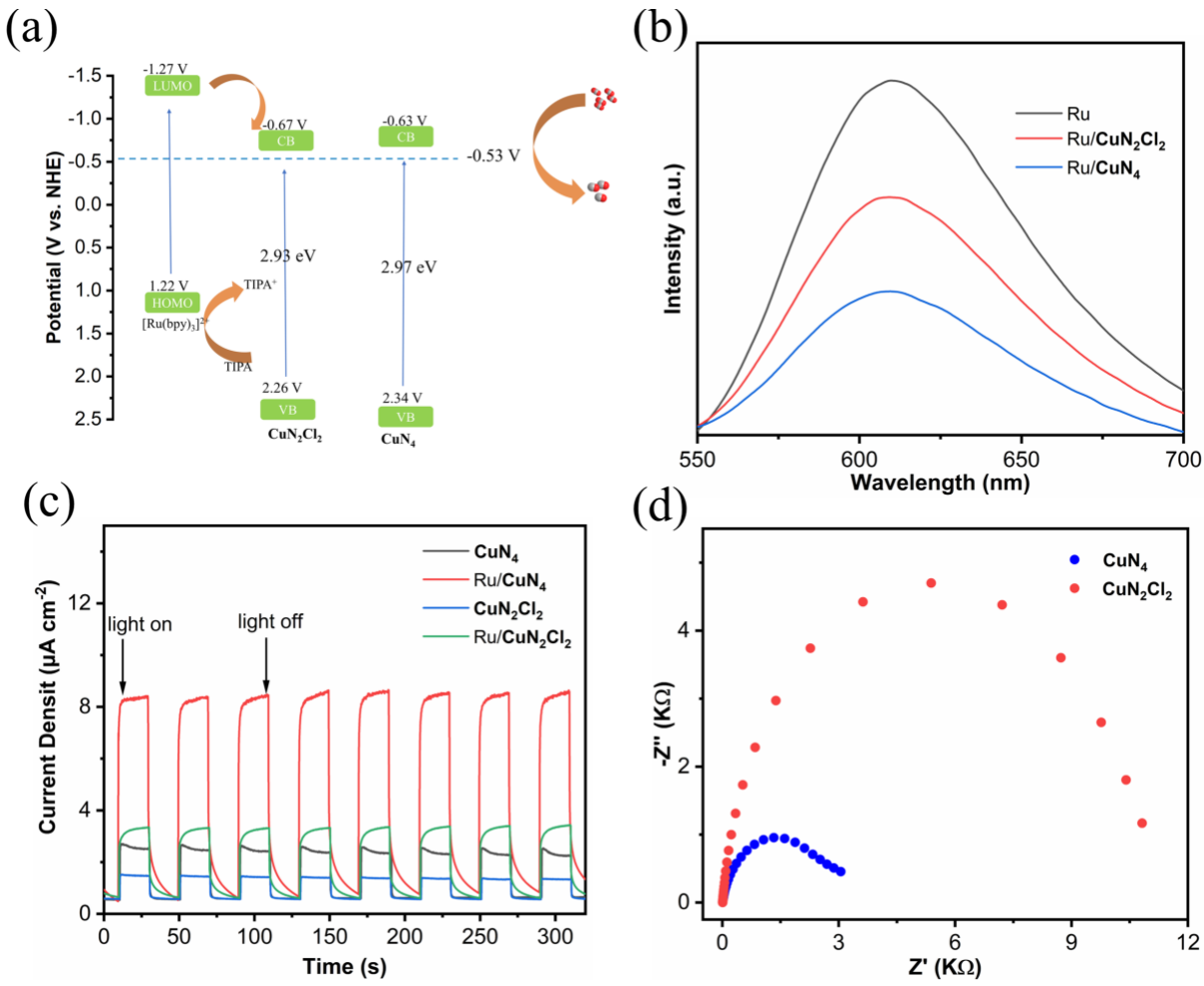

Fig. S8 (a) Band structure and positions of Cu-MOFs and $[Ru(bpy)_3]^{2+}$. (b) Steady state fluorescence spectra of $[Ru(bpy)_3]Cl_2·6H_2O$ upon addition of Cu-MOFs (λ_{ex} = 420 nm). (c) Transient photocurrent response of Cu-MOFs and Cu-MOFs with $[Ru(bpy)_3]Cl_2·6H_2O$. (d) EIS Nyquist plots of Cu-MOFs.

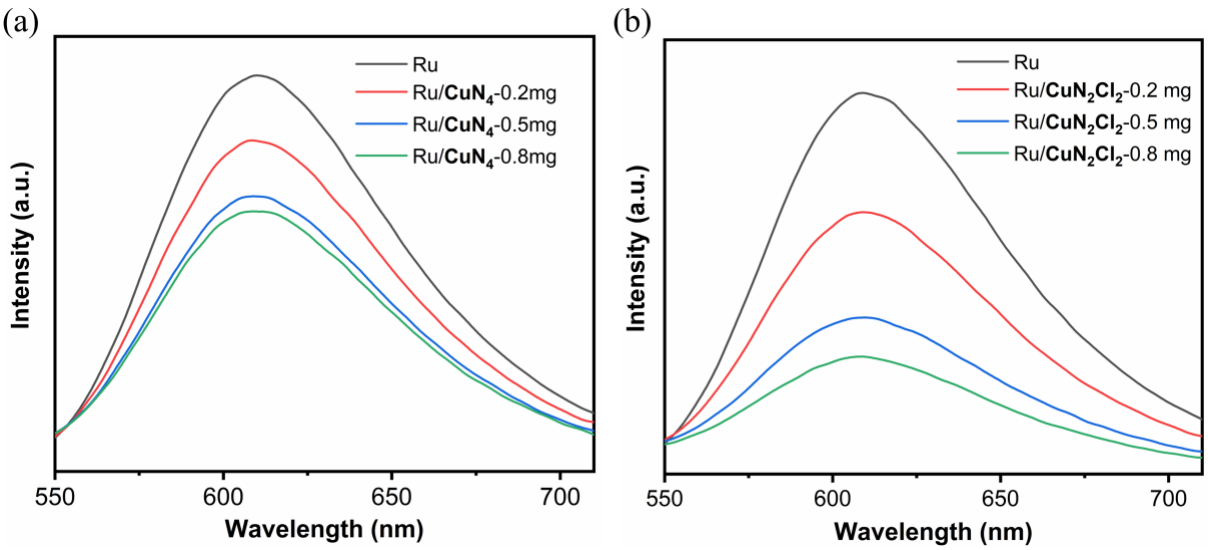

Fig. S9 Steady state fluorescence spectra of $[Ru(bpy)_3]Cl_2$ upon the addition of increasing amounts of **CuN_4** (a) and **CuN_2Cl_2** (b) (λ_{ex} = 420 nm).

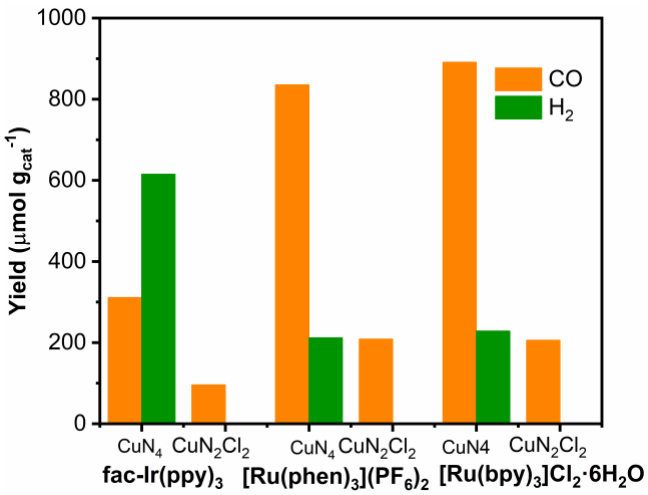

Fig. S10 Photocatalytic CO_2 reduction results using varied photosensitizers.

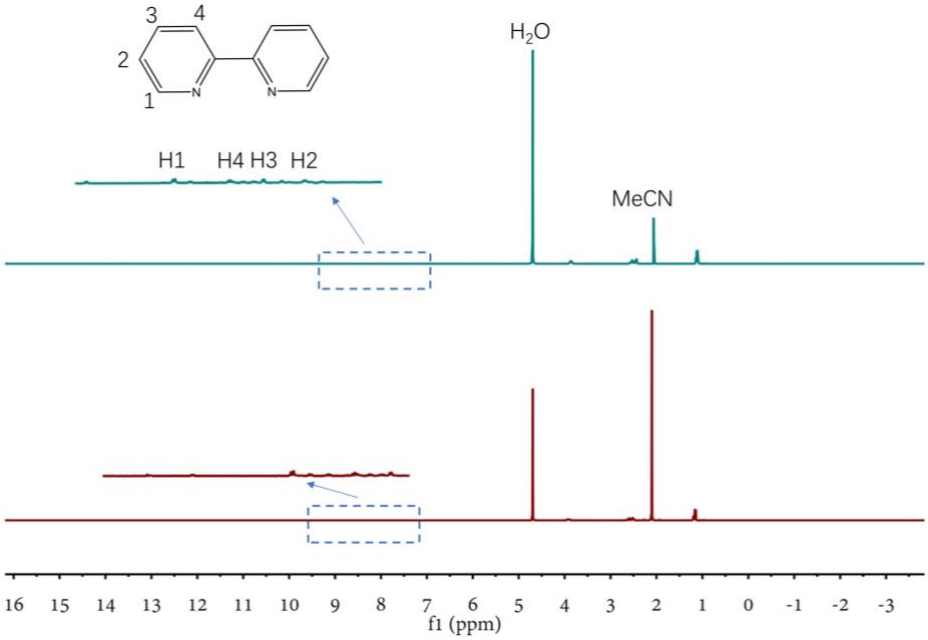

Fig. S11 ^{1}H NMR spectra in D_2O for the liquid phase after the photocatalytic experiments. **CuN_2Cl_2** (up), **CuN_4** (bottom).

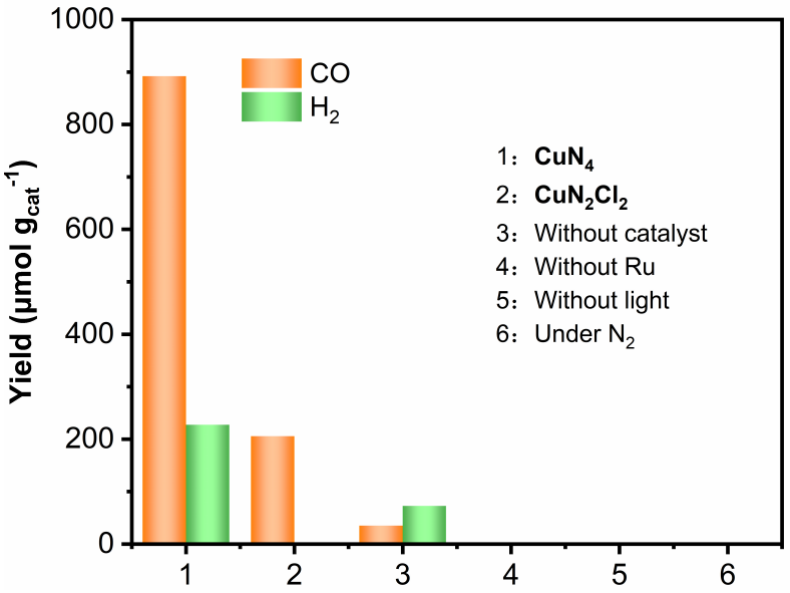

Fig. S12 Photocatalytic CO_2 reduction results under varied reaction conditions.

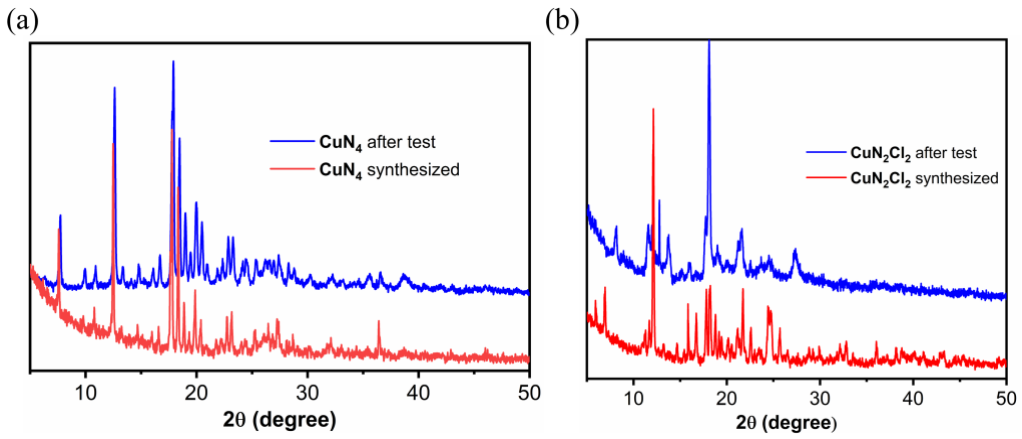

Fig. S13 PXRD of **CuN_4** (a) and **CuN_2Cl_2** (b) after the photocatalytic experiments.

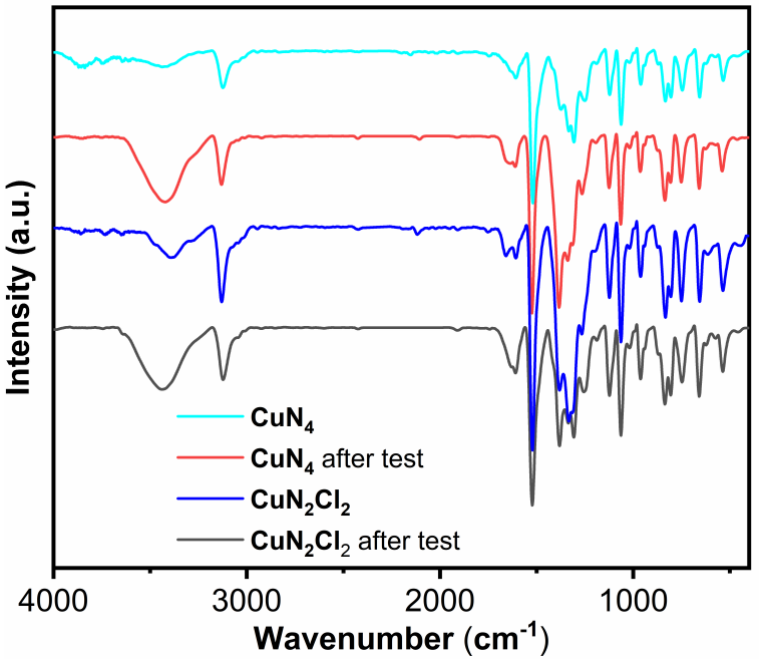

Fig. S14 FT-IR spectra of **CuN_4, CuN_2Cl_2** and Cu-MOFs after the photocatalytic experiments.

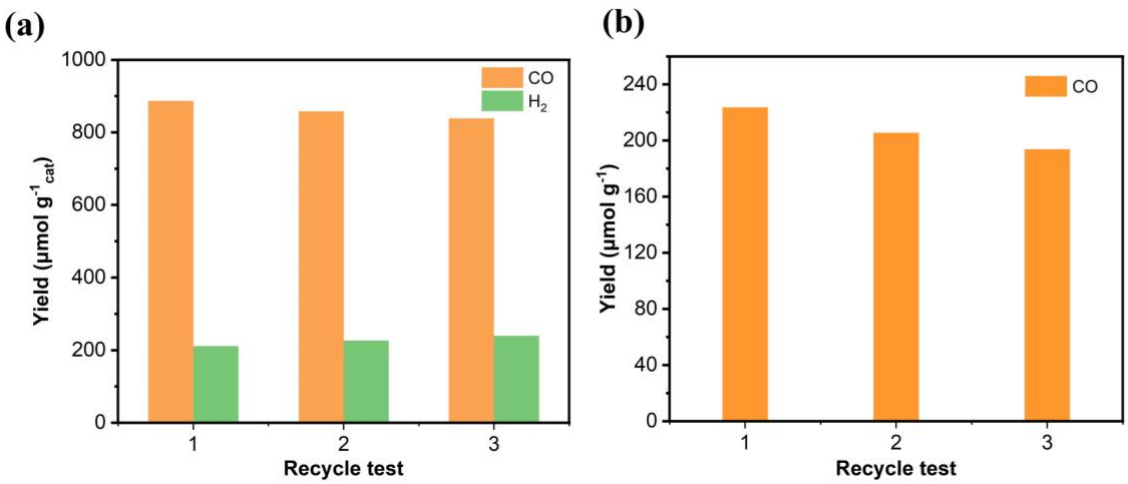

Fig. S15 Recyclability of **CuN_4** (a) and **CuN_2Cl_2** (b).

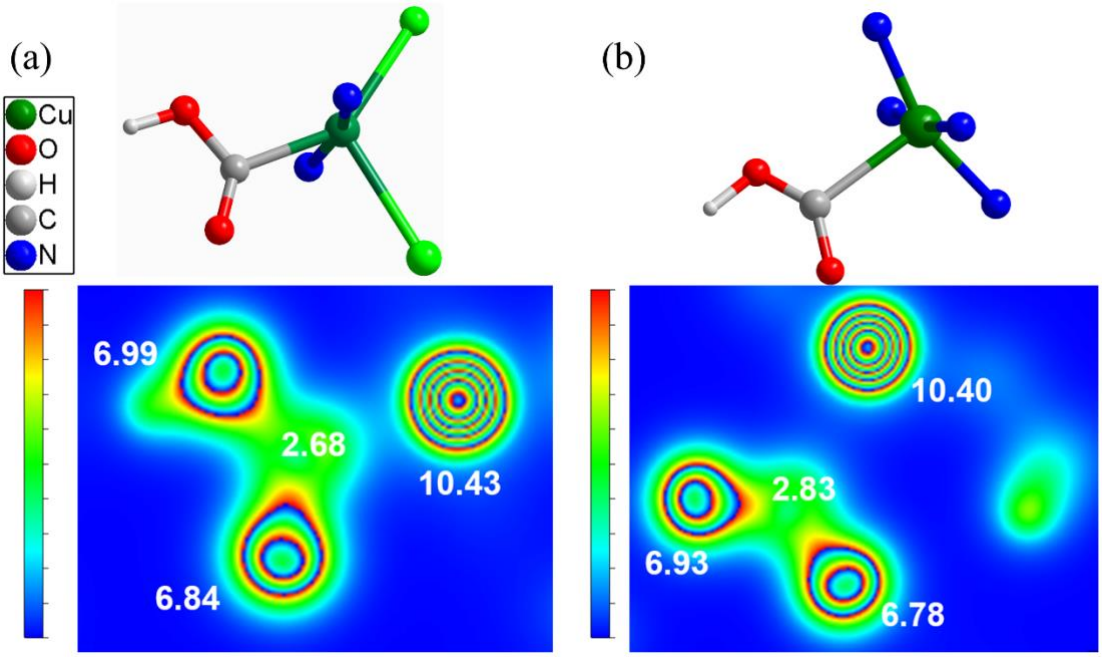

Fig. S16 Optimized structures (upper) and slice of the calculated charge densities (below) of **CuN_2Cl_2** (a) and **CuN_4** (b) with adsorbed *COOH. Bader partial atomic charges are labeled by the white numbers.

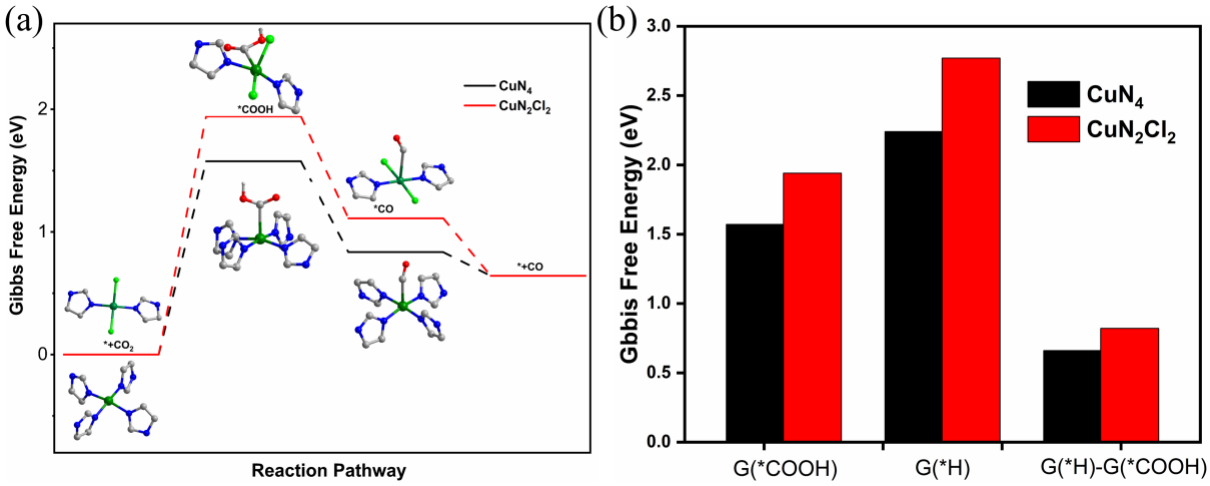

Fig. S17 (a) Calculated Gibbs free energy ΔG diagrams of CO_2 to CO of **CuN_2Cl_2** and **CuN_4**, respectively. (b) Calculated Gibbs free energy profile of G(*COOH), G(*H) and G(*H)-G(*COOH) on **CuN_2Cl_2** and **CuN_4**.[8,9]

Table S1. Crystal data and structural refinement data for **CuN_4** and **CuN_2Cl_2**

	CuN_4	**CuN_2Cl_2**
formula	$C_{76}H_{65}Cu_2N_{20}O_{16.5}$	$C_{40}H_{33}Cl_4Cu_2N_9O$
formula weight	1649.56	924.62
crystal system	tetragonal	monoclinic
space group	$P4_3$	$P2_1/n$
a (Å)	19.7601(8)	15.805(4)
b (Å)	19.7601(8)	9.323(2)
c (Å)	19.9303(11)	27.137(7)
β (deg)	90	99.835(10)
V (Å^3)	7782.0(8)	3939.7(17)
Z	4	4
Dc (g cm^{-3})	1.408	1.529
μ (mm^{-1})	3.387	1.394
F(000)	3404	1840.0
no. of reflections collected	60540	27919
no. of unique reflections	13904	7268
goodness of fit	1.052	1.054
largest difference peak/hole (e Å^{-3})	0.34/-0.42	0.57/-0.73
R_1[a] [I > 2σ(I)]	0.0786	0.0712
wR_2[b] [I > 2σ(I)]	0.1977	0.1489

[a]$R_1 = \sum||F_0| - |F_c||/\sum|F_0|$. [b]$wR_2 = |\sum w(|F_0|^2 - |F_c|^2)|/\sum|w(F_0)^2|^{1/2}$, where $w = 1/[\sigma^2(F_0^2) + (aP)^2 + bP]$. $P = (F_0^2 + 2F_c^2)/3$.

Table S2. Selected bond lengths (Å) and bond angles (°) for **CuN$_4$**.

Cu1-O1	2.391(8)	Cu2-N4#3	2.020(10)
Cu1-N1	2.005(9)	Cu2-N8	2.025(9)
Cu1-N6#1	2.021(9)	Cu2-N9	2.001(9)
Cu1-N11#2	2.031(9)	Cu2-N15#4	1.993(11)
Cu1-N13	2.011(10)	Cu2-O2	2.380(8)
N1-Cu1-O1	92.3(3)	N4#3-Cu2-O2	94.5(3)
N1-Cu1-N6#1	179.0(4)	N4#3-Cu2-N8	175.0(4)
N1-Cu1-N11#2	90.6(4)	N9-Cu2-N4#3	88.3(4)
N1-Cu1-N13	88.9(4)	N8-Cu2-O2	90.4(3)
N6#1-Cu1-O1	88.7(4)	N9-Cu2-O2	92.8(3)
N6#1-Cu1-N11#2	89.2(4)	N9-Cu2-N8	90.5(4)
N13-Cu1-O1	94.6(3)	N15#4-Cu2-O2	90.0(4)
N13-Cu1-N6#1	91.3(4)	N15#4-Cu2-N8	89.0(4)
N13-Cu1-N11#2	174.9(4)	N15#4-Cu2-N9	177.1(4)
N11#2-Cu1-O1	90.5(3)	N15#4-Cu2-N4#3	91.9(4)

Symmetry transformations used to generate equivalent atoms:

#1 +X, +Y, -1+Z; #2 +X, 1+Y, +Z; #3 +X, -1+Y, +Z; #4 +X, +Y, 1+Z;

Table S3. Selected bond lengths (Å) and bond angles (°) for **CuN_2Cl_2**.

Cu1-Cl1	2.291(2)	Cu2-Cl3	2.254(2)
Cu1-Cl2	2.339(2)	Cu2-Cl4	2.252(2)
Cu1-N1	1.974(5)	Cu2-N5#2	2.002(5)
Cu1-N3#1	1.977(5)	Cu2-N7	2.017(5)
Cu1-N9	2.400(7)		
Cl1-Cu1-Cl2	142.38(8)	Cl1-Cu1-N9	108.4(2)
Cl2-Cu1-N9	109.2(2)	N1-Cu1-Cl1	91.03(18)
N1-Cu1-Cl2	91.85(16)	N1-Cu1-N3#1	171.0(2)
N1-Cu1-N9	83.5(2)	N3#1-Cu1-Cl1	92.30(17)
N3#1-Cu1-Cl2	90.64(16)	N3#1-Cu1-N9	87.4(2)
Cl4-Cu2-Cl3	163.91(9)	N5#2-Cu2-Cl3	89.55(18)
N5#2-Cu2-Cl4	88.19(18)	N5#2-Cu2-N7	171.5(2)
N7-Cu2-Cl3	92.75(17)	N7-Cu2-Cl4	91.81(17)

Symmetry transformations used to generate equivalent atoms:

#1 -1/2+X, 3/2-Y, 1/2+Z; #2 1/2+X, 1/2-Y, -1/2+Z;

Table S4. Hydrogen bonding data of **CuN_2Cl_2**.

D-H ···A	d(D-H) (Å)	d(H···A) (Å)	d(D···A) (Å)	D-H ···A (°)
C22-H22···Cl1#1	0.95	2.81	3.673(7)	151
C39-H39A···Cl2#2	0.98	2.76	3.721(9)	167
C39-H39C···Cl2#3	0.98	2.78	3.697(9)	157

Symmetry transformations used to generate equivalent atoms:

#1 1-X, 1-Y, 1-Z; #2 1-X, 2-Y, 1-Z; #3 X, 1+Y, Z;

Table S5. The member atoms of conjugated rings for **CuN_2Cl_2**. (CgI = plane number I).

CgI	Ring member atoms					
Cg1	N1	N2	C1	C2	C3	
Cg2	N3	N4	C17	C18	C19	
Cg3	N5	N6	C20	C21	C22	
Cg4	N7	N8	C36	C37	C38	
Cg5	C4	C5	C6	C7	C8	C9
Cg6	C11	C12	C13	C14	C15	C16
Cg7	C23	C24	C25	C26	C27	C28
Cg8	C30	C31	C32	C33	C34	C35

Table S6. The Cg-Cg distances (Å) between ring centroids for **CuN_2Cl_2 (**face-to-face**)**.

	CgI->CgJ	Distance		CgI->CgJ	Distance
1	Cg2->Cg5#3	4.698(4)	8	Cg5->Cg7#8	4.458(4)
2	Cg2->Cg7#3	4.951(4)	9	Cg6->Cg5#3	4.868(4)
3	Cg2->Cg7#2	4.720(4)	10	Cg6->Cg6#3	4.886(4)
4	Cg3->Cg2#4	4.692(4)	11	Cg6->Cg8#8	4.627(4)
5	Cg4->Cg4#6	4.863(5)	12	Cg7->Cg5#8	4.458(4)
6	Cg4->Cg4#6	4.545(5)	13	Cg8->Cg3#5	4.860(4)
7	Cg5->Cg2#2	4.698(4)	14	Cg8->Cg6#8	4.627(4)

Symmetry transformations used to generate equivalent atoms:

#1 1-X, 1-Y, 1-Z; #2 3/2-X, 1/2+Y, 1/2-Z; #3 3/2-X, -1/2+Y, 1/2-Z; #4 -1+X, Y, Z; #5 1/2-X, -1/2+Y, 1/2-Z; #6 1-X, -Y, -Z; #7 1-X, 1-Y, -Z; #8 X, Y, Z;

Table S7. The distance of H to Cg distances (Å) for **CuN_2Cl_2** (edge-to-face).

X--H(I)···Cg(J)	Distances	X--H(I)···Cg(J)	Distances
C6-H6->Cg6#1	2.76	C27-H27->Cg2#3	2.83
C20-H20->Cg8#2	3.00	C31-H31->Cg6#3	2.82
C25-H25->Cg2#1	2.89	C39-H39B->Cg3#4	2.91

Symmetry transformations used to generate equivalent atoms:

#1 3/2-X, 1/2+Y, 1/2-Z; #2 1/2-X, 1/2+Y, 1/2-Z; #3 3/2-X, -1/2+Y, 1/2-Z; #4 1-X, 2-Y, 1-Z;

Table S8. The distance of Cl atom to Cg distances (Å) for **CuN_2Cl_2**.

Y--X(I) ···Cg(J)	Distances
Cu1-Cl1->Cg7#1	3.807(3)
Cu2-Cl3->Cg1#2	3.651(4)
Cu2-Cl4->Cg4#3	3.963(4)

Symmetry transformations used to generate equivalent atoms:

#1 1/2+X, 3/2-Y, 1/2+Z; #2 3/2-X, -1/2+Y, 1/2-Z; #3 1-X, -Y, -Z;

Table S9. Photocatalytic CO_2 reduction for varied samples under xenon lamp irradiation.

Catalytic system	Solvent	Light	Sacrificial Agent	Yield of CO(μmol g^{-1}) / time (h)	Ref.
CuN_4	MeCN / H_2O = 4:1	AM 1.5 G	TIPA	891/5	**This work**
CuN_2Cl_2	MeCN / H_2O = 4:1	AM 1.5 G	TIPA	205.8/5	**This work**
MOF-Cu	MeCN / H_2O = 13:1	300 W Xe lamp	TIPA	408/6	10
CUST-804	MeCN / H_2O = 4:1	λ> 420	TEOA	2710/1	11
BIF-105	MeCN / H_2O = 4:1	λ> 420	TEOA	5598/6	12
MOF-Ni	MeCN / H_2O = 4:1	300 W Xe lamp	TEOA	2388/4	13
MOF-Co	MeCN / H2O = 4:1	300 W Xe lamp	TEOA	4988/4	13
NJU-Bai 61	H_2O / TEA= 9:1	300 < λ < 2500	TEA	16/4	14
ZIF-67_3	MeCN / H_2O = 4:1	λ > 400	TEOA	14250/3.8	15
[Mn(L)Cl]·DMF	/	300 W Xe lamp	TEOA	85.8/6	16
[Fe(L)Cl]·DMF	/	300 W Xe lamp	TEOA	189.6/6	16
L= 6,60-((1E,10E)-(ethane-1,2-diylbis(azanylylidene))bis(methanylylidene))bis(3-(pyridin-4-yl) phenol)					

References

1. K. Y. Kim, S. H. Jung, J. H. Lee, S. S. Lee and J. H. Jung, *Chem. Commun.*, 2014, **50**, 15243-15246.
2. N. Sinha, L. Stegemann, T. T. Tan, N. L. Doltsinis, C. A. Strassert and F. E. Hahn, *Angew. Chem. Int. Ed*., 2017, **56**, 2785-2789.
3. SAINT, *Bruker AXS*, Inc., Madison WI2001.
4. G. M. S. Sheldrick, *University of Gottingen,* Gottingen, Germany, 2003.
5. G. M. Sheldrick, *Acta Crystallogr. C Struct. Chem.*, 2015, **71**, 3-8.

6. Y. Zhou, S. T. Liu, Y. M. Gu, G. H. Wen, J. Ma, J. L. Zuo and M. N. Ding, *J. Am. Chem. Soc.*, 2021, **143**, 14071-14076.
7. A. A. Peterson, F. Abild-Pedersen, F. Studt, J. Rossmeisl and J. K. Nöskov, *Energy Environ. Sci*., 2020, **3**, 1311-1315.
8. C. C. Xu, X. Zhi, A. Vasileff, D. Wang, B. Jin, Y. Jiao, Y. Zheng, and S. Z. Qiao, *Small Struct.,* 2021, **2**, 2000058.
9. H. H. Chen, X. Guo, X. D. Kong, Y. L. Xing, Y. Liu, B. L. Yu,Q. X. Li, Z. G. Geng, R. Si and J. Zeng, *Green Chem.*, 2020, **22**, 7529-7536.
10. X. K. Wang, J. Liu, L. Zhang, L. Z. Dong, S. L. Li, Y. H. Kan, D. S. Li and Y. Q. Lan, *ACS Catal.*, 2019, **9**, 1726-1732.
11. X. Han, Y. J. Chu, M. Dong, W. Chen, G. Ding, L. L. Wen, K. Z. Shao, Z. Su, M. Zhang, X. Wang and G. G. Shan, *Inorg. Chem.*, 2022, **61**, 5869-5877.
12. Y. M. Wang, H. X. Zhang, and J. Zhang, *Dalton. Trans.,* 2021, **50**, 490.
13. J. H. Zhang, Y. C. Wang, H. J. Wang, D. C Zhong and T. B. Lu, *Chinese Chem. Lett.*, 2022, **33**, 2065-2068.
14. Y. Gao, L. Zhang, Y. Gu, W. Zhang, Y. Pan, W. Fang, J. Ma, Y. Q. Lan and J. Bai, *Chem. Sci.*, 2020, **11**, 10143-10148.
15. M. Wang, J. X. Liu, C. M. Guo, X. Gao, C. S. Gong, Y. H. Wang, B. Liu, X. X. Li, G. G. Gurzadyan and L. C. Sun, *J. Mater. Chem. A*, 2018, **6**, 4768-4775.
16. Y. Liu, J. H. Guo, X. Y. Dao, X. D. Zhang, Y. Zhao and W. Y. Sun, *Chem. Commun.*, 2020, **56**, 4110-4113.